

# Nucleated Conformational Conversion and the Replication of Conformational Information by a Prion Determinant

Tricia R. Serio,<sup>1\*</sup> Anil G. Cashikar,<sup>2\*</sup> Anthony S. Kowal,<sup>2</sup>  
George J. Sawicki,<sup>2</sup> Jahan J. Moslehi,<sup>2</sup> Louise Serpell,<sup>4</sup>  
Morton F. Arnsdorf,<sup>3</sup> Susan L. Lindquist<sup>1,2†</sup>

Prion proteins can serve as genetic elements by adopting distinct physical and functional states that are self-perpetuating and heritable. The critical region of one prion protein, Sup35, is initially unstructured in solution and then forms self-seeded amyloid fibers. We examined *in vitro* the mechanism by which this state is attained and replicated. Structurally fluid oligomeric complexes appear to be crucial intermediates in *de novo* amyloid nucleus formation. Rapid assembly ensues when these complexes conformationally convert upon association with nuclei. This model for replicating protein-based genetic information, nucleated conformational conversion, may be applicable to other protein assembly processes.

In *Saccharomyces cerevisiae*, the prion element [*PSI*<sup>+</sup>] causes heritable changes in translational fidelity (1) through self-perpetuating changes in the state of Sup35 (2–4), a component of the translation termination factor. Together the glutamine-rich NH<sub>2</sub>-terminal (N) and highly charged middle (M) regions of Sup35 adopt distinct physical states (either soluble or insoluble higher order complexes), and these produce the distinct translational activities of [*psi*<sup>-</sup>] and [*PSI*<sup>+</sup>] strains (3, 4). Sup35 complexes replicate their conformational state, and thereby perpetuate [*PSI*<sup>+</sup>], by converting newly made Sup35 to the same state (3). *In vitro*, highly ordered NM complexes (fibers) promote the conversion of soluble NM to the same state, closely modeling the *in vivo* process (5). Lysates of [*PSI*<sup>+</sup>], but not [*psi*<sup>-</sup>], cells accelerate NM polymerization (5, 6), and mutations that enhance or inhibit [*PSI*<sup>+</sup>] propagation enhance or inhibit NM conversion (5, 7, 8) in a complementary way. But the conformational conversion mechanism that replicates the protein-based genetic information of [*PSI*<sup>+</sup>] is unknown.

The three most prominent models proposed for self-propagating changes in protein state fundamentally differ in the role that preexisting polymers play in converting soluble, S-state protein to assembled, A-state protein and in the

nature of the rate-limiting step (Fig. 1). For templated assembly (TA) (9, 10), A-state complexes act as templates for S→A conformational conversion (the rate-limiting step) during assembly. Conformational conversion is also rate-limiting for monomer-directed conversion (MDC) (11), but S monomers convert to A monomers in solution, and assembly is a consequence, not a cause, of conversion. For nucleated polymerization (NP) (12–14), the S and A states are in equilibrium in solution, but the A state is rare and unstable. The rate-limiting step is not conformational conversion but chance association of a sufficient number of A monomers to form a stable, polymerization-competent nucleus. A-state monomers, generated by the S↔A equilibrium, are stabilized by joining the nucleus, as in seeded crystallization.

**Nucleation by solid-phase A-state protein.** To test these models for NM conformational conversion and assembly, we first characterized the A state. During fibrillization, NM became resistant to cleavage with proteases: Chymotrypsin resistance appeared concomitant with assembly (Fig. 2A); a modest V8 resistance appeared later (Fig. 2B). Because chymotrypsin cleavage sites are restricted to N, and V8 sites to M, these observations support the hypothesis that N directs fiber formation with M on the outside (5). By x-ray diffraction, NM fibers had a prototypical amyloid, cross- $\beta$  structure (Fig. 2C) (15). Fibers resisted solubilization in 8 M urea and 2% (w/v) SDS at room temperature (Fig. 2D), but were solubilized in 2% (w/v) SDS when boiled for 10 min. Fibers were also rigid and easily fractured into short pieces by sonication (Fig. 2, E and F).

Sonication greatly enhanced the nucleating activity of NM fiber solutions (Fig. 3 and

Table 1) (16, 17). It did not do so by increasing the concentration of a soluble accelerant, because nucleating activity was removed by centrifugation at 100,000g for 10 min (17). Nor did it change the biochemical nature of the protein (18). Furthermore, fracturing the fibers did not simply keep nucleating material in suspension; even unsonicated fibers remained in suspension during these experiments (17). When fresh NM was added, fragments converted to long, unclumped fibers (17). Thus, assembled protein is the species that accelerates conversion—eliminating MDC for NM—and fiber ends, rather than lateral surfaces, appear to be crucial for nucleation (seeding).

**Simultaneous acquisition of structure and assembly.** To investigate the relation between structural conversion and assembly, we simultaneously analyzed (i) assembly, by sedimentation, light scattering, transmission electron microscopy (TEM), and atomic force microscopy (AFM); (ii) structural change, by circular dichroism (CD), limited proteolysis, and dye binding; and (iii) stability, by SDS solubility. In unseeded reactions, the half-point of assembly, determined by centrifugation and light scattering, was reached at ~50 hours (Fig. 3). By ~50 hours, NM had gained 50% of its maximum ability to bind Congo red (CR) (Fig. 3); the random-coil signal in the CD spectrum (approaching 200 nm) was substantially reduced (17), fibers became abundant by microscopy (17), and nearly 50% of the protein had become resistant to cleavage with chymotrypsin (19) and insoluble in 2% (w/v) SDS (Fig. 3) (20). 8-Anilino-1-naphthalene sulfonate (ANS) fluorescence (21) also changed during fibrillization. It did not reveal, as it commonly does, a structural intermediate, but rather the accessibility of a hydrophobic environment in mature NM fibers (22). ANS fluorescence reached a maximum at the same time as other traits of the A state (Fig. 3).

A similar congruence between the acquisition of structure and assembly was observed in seeded reactions, both with unfractured and with sonicated fibers (Fig. 3). The coincident acquisition of all A-state structural traits in reactions occurring over vastly different time frames indicates that the A structure is either attained concomitantly with polymerization, as predicted by TA, or is too rare to detect in solution during any of these time courses.

**Kinetic analysis of the lag and assembly phases.** We next examined the concentration dependence of the lag phase, during which nuclei form, and the assembly phase, in which unpolymerized protein joins these nuclei (23, 24). The NP and TA models make different predictions for the concentration dependence of both phases.

Nucleation by NP depends on the number of A-state monomers that must come together

<sup>1</sup>Department of Molecular Genetics and Cell Biology, <sup>2</sup>Howard Hughes Medical Institute, <sup>3</sup>Section of Cardiology, Department of Medicine, University of Chicago, Chicago, IL 60637, USA. <sup>4</sup>Neurobiology Division, MRC Centre, Laboratory of Molecular Biology, Cambridge CB2 2QH, UK.

\*These authors contributed equally to this work.

†To whom correspondence should be addressed. E-mail: s-lindquist@uchicago.edu

to form a stable nucleus. The lag phase, therefore, varies exponentially with that number (14). Nucleation by TA presumably depends on the rate of S→A conversion and thus should vary directly with concentration. The lag phase for polyhistidine-tagged NM varies little with protein concentration (5, 7). Because this tag affects polymerization (see below), we investigated the effects of concentration on the lag phase using unmodified NM. Over a 500-fold range (0.1 to 50  $\mu\text{M}$ ), a lag phase was detected (25), and even at the highest concentration this phase was  $\sim 20$  hours, demonstrating a rate-limiting step in nucleus formation (Fig. 4A). However, the lag phase varied over this concentration range by less than 10-fold (Fig. 4A), a conundrum for either the NP or the TA model.

Assembly rates, according to NP, are determined by the pace at which soluble A-state protein is generated by the S $\leftrightarrow$ A equilibrium and collides with preformed nuclei (14). The concentration of A and the rate of assembly should increase directly with total soluble protein. For TA, assembly is limited by the rate at which S-state protein, interacting with an A-state nucleus, is conformationally converted to regenerate the nucleating surface. Only in the extreme case where nucleating surfaces are in excess will assembly rates vary with the concentration of soluble protein (26).

Post-lag phase assembly times in unseeded reactions were constant over a broad range of concentrations but increased sharply below 5  $\mu\text{M}$  (Fig. 4B). In these reactions, at the end of the lag phase,  $>90\%$  of the protein was soluble and structurally unconverted (Fig. 3). Similarly, in seeded reactions containing a fixed quantity of soluble NM (5  $\mu\text{M}$ ) and different quantities of sonicated fibers, the rate of conformational change was proportional to the quantity of fibers added only until the seed concentration reached 1% (w/w) (Fig. 4C). At this point, soluble protein was in excess over fiber ends by  $\sim 50,000$ -fold (17). These experiments reveal a second

conundrum for either NP or TA: Assembly rates showed little concentration dependence over a broad range but reached a limit when monomer concentrations remained in vast excess over polymerization surfaces.

**Evidence for an oligomeric intermediate in nucleation and assembly.** Evidence for an intermediate in fiber formation, which might explain these conundrums, was obtained when solutions of NM were preincubated for various times before the addition of fibers. When fibers (0.15% w/w) were added immediately to freshly solubilized NM, assembly proceeded as a first-order reaction (Fig. 4D); when they were added to NM solutions after an 8-hour preincubation, the reaction proceeded in two stages (Fig. 4D), with an initial phase 40-fold faster than the second phase. The contribution of the fast phase to the assembly process increased with the length of the preincubation, until the preincubating solutions themselves had initiated fiber formation (27). Thus, an intermediate accumulated during the lag phase that promoted rapid NM assembly and was quickly consumed once assembly began.

The fast phase of assembly was not observed when fibers were added to NM solutions preincubated for 8 hours in the same buffer but with 1 M NaCl (27). The CD spectra of NM solutions was similar in 1 and 0.15 M NaCl, suggesting that secondary structure was not substantially altered (27). However, solutions scattered more light in 0.15 M than in 1 M NaCl immediately after NM was solubilized (Fig. 4E).

This early signal was due not to the formation of fibers (Fig. 3) but to oligomeric complexes (17). Notably, salt and other conditions (4°C, His<sub>10</sub> tag) that increased or decreased initial light scattering (Fig. 4E) increased or decreased the rate of fibrillization in a complementary way (Fig. 4F), providing independent evidence that nucleus formation and assembly are mediated by an oligomeric intermediate.

If fibrillization were mediated by a complex composed of a defined number of subunits that interact through specific surfaces, the rate should be exponentially dependent on soluble protein concentration. Curiously, the equilibrium between monomers and oligomers was not affected by concentration in the range of our experiments. Initial light scattering from NM in physiologic salt increased in simple proportion to concentration over a 100-fold range (0.3 to 35  $\mu\text{M}$ ) (27), and oligomers were always much less abundant than monomers (28).

**Structural and morphological characterization of NM oligomers.** During assembly, spherical, variably sized oligomeric complexes were detected by several types of microscopy (Fig. 5). By scanning transmission electron microscopy (STEM), their mass was  $1.6 \times 10^6$  daltons (SD = 0.8,  $n = 359$ ), corresponding to complexes of  $\sim 20$  to 80 NM monomers (Fig. 5, B and C). Notably, fibers, which appeared smooth by TEM (Fig. 2E), were shown by AFM to be composed of segments with an average height of  $\sim 4$  nm (Fig. 5, A, D, and E). Most complexes were in the range of 2 to 4 nm

**Table 1.** Time course reactions with 5  $\mu\text{M}$  NM alone (unseeded) or in the presence of 2% (w/w) intact (seeded) or sonicated fibers either unrotated or rotated as for Fig. 2, quantified by CR binding as for Fig. 3.  $L_T$ , lag time;  $A_{T/1/2}$ , 50% assembly time.

	Unseeded		Unsonicated seed	Sonicated seed
	$L_T$ (hours)	$A_{T/1/2}$ (hours)	$A_{T/1/2}$ (hours)	$A_{T/1/2}$ (hours)
Unrotated	33	29	3	0.4
Rotated	0.33	0.2	0.2	0.3

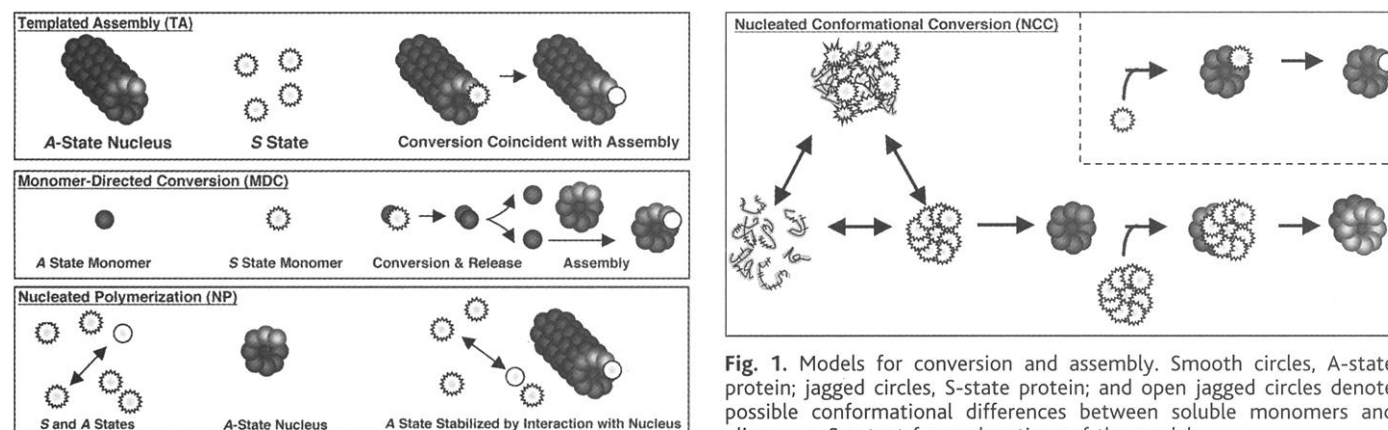


**Fig. 1.** Models for conversion and assembly. Smooth circles, A-state protein; jagged circles, S-state protein; and open jagged circles denote possible conformational differences between soluble monomers and oligomers. See text for explanations of the models.

(17), suggesting that fibers might form by assembly of these complexes. Larger complexes, which appeared ineligible for assembly, were also observed (Fig. 5D, arrow).

Oligomers often interacted with each other and with fiber ends (Fig. 5, B, C, and G to I, arrows). These associations were more frequent in reactions with His<sub>10</sub>-tagged NM (17), which formed fibers more rapidly than unmodified NM (Fig. 4F). Oligomers seemed deformed by their interactions (Fig. 5, B, C, and G to I), indicating a malleability not characteristic of fibers. Oligomers were sticky and adhered more efficiently to mica and quartz than did fibers. They were also more readily disrupted (29). Together these

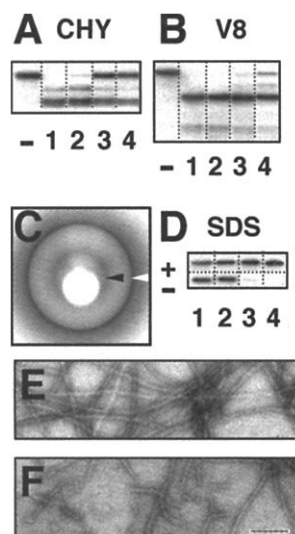


**Fig. 2.** Defining the A state for NM. NM was purified as described (40). (A) Chymotrypsin (CHY) sensitivity. NM (5  $\mu$ M) in CRBB [5 mM potassium phosphate (pH 7.4), 0.15 M NaCl] after rotation on a roller drum at 60 rpm for 0 (lane 1), 0.5 (lane 2), 1.25 (lane 3), or 2.5 hours (lane 4), digested with CHY (1/250 w/w) at 37°C for 15 min. Undigested (–) and digested samples were analyzed by SDS–polyacrylamide gel electrophoresis (PAGE), electroblotted to Immobilon-P (Millipore), and immunoblotted with a monospecific polyclonal rabbit antiserum to Sup35 (3) and <sup>125</sup>I–protein A. No changes in the pattern were detected with gels stained with Coomassie Brilliant Blue. (B) V8 sensitivity. Reactions as in (A) with endoproteinase Glu-C (V8; 1/50 w/w). (C) X-ray diffraction. Fibers (confirmed by TEM) were assembled in CRBB at 10 mg/ml, dialyzed against distilled, deionized water, and subjected to x-ray diffraction (75). Meridian reflections at 4.7 Å (black arrowhead), equatorial reflections at 9 Å (white arrowhead). (D) SDS solubility. SDS was added to 2% (w/v) to 20- $\mu$ l samples of NM (5  $\mu$ M) as in (A), incubated at 100°C (+) or 25°C (–) for 10 min, and analyzed as described in (A). TEM images of unsonicated (E) and sonicated (F) NM fibers. Solutions of NM fibers (5  $\mu$ M) were sonicated for 15 s at 4°C with a Dynatech Industries sonic dismembrator (Model 302) fitted with a microtip. Protein (5  $\mu$ l of a 5  $\mu$ M solution) was analyzed as described (5). Bar (E and F), 100 nm.

observations indicate that oligomers are less rigidly structured than fibers.

**Rotation accelerates both the lag and assembly phases.** An on-pathway role for oligomers is supported by the effects of modest agitation. Both the lag phase and the assembly phase were accelerated  $\sim$ 100-fold when reactions were rotated at 60 rpm (Table 1). Rotation

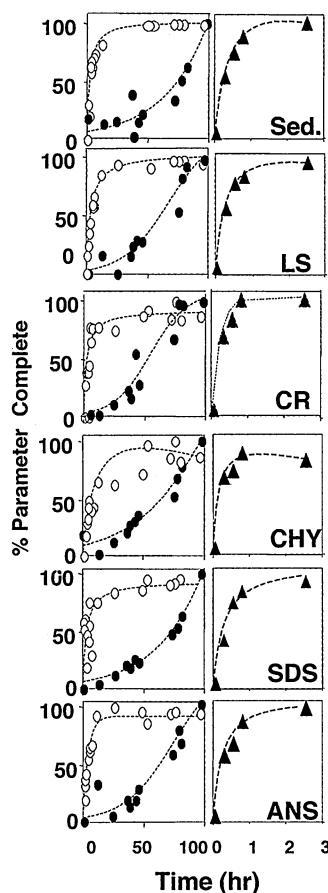


**Fig. 3.** Characterization of NM assembly. Time courses of NM (5  $\mu$ M) assembly in CRBB. Unseeded reactions (●), reactions seeded with unsonicated fibers (2% w/w) (○), reactions seeded with sonicated fibers (2% w/w) (▲). An equal amount of sample was transferred into separate tubes for each time point. Sed, sedimentation at 100,000g for 10 min at 4°C in a Beckman TLA-100 rotor. Protein remaining in the supernatant was analyzed by SDS-PAGE and immunoblotting as in Fig. 2 and quantified by PhosphorImager. LS, light scattering (90°, 500 nm) expressed as a percentage of the value at the end of fiber assembly. CR, binding was determined as described (5). CHY, chymotrypsin resistance as in Fig. 2A, expressed as a percentage of the total protein, quantified by PhosphorImager analysis. SDS, insolubility determined as in Fig. 2D, expressed as a percentage of total protein, quantified by PhosphorImager. ANS, fluorescence intensity of ANS at the  $\lambda_{\text{max}}$  of 490 nm, expressed as a percentage of the final value. Solutions of 5  $\mu$ M NM and 10  $\mu$ M ANS were excited at 370 nm, and fluorescence spectra were recorded with a 5-nm bandwidth. Dotted lines are guidelines only, not evaluated fits.

at a slower speed produced a more modest increase in rate, but again both phases were affected similarly (8). Rotation did not fracture fibers to create new ends (30), as previously postulated (7). We suggest that rotation accelerates polymerization by dissociating overly large complexes and/or increasing the collision of eligible complexes with each other and with fiber ends. Indeed, rotation eliminated the strong concentration dependence of assembly below 5  $\mu$ M (Fig. 4B).

**Rate-limiting conversion.** Because rotation and seeding accelerate NM assembly by different mechanisms (altering fluid dynamics versus providing preformed ends for polymerization), combining the two might be expected to produce an even greater increase in rate. Rotation did increase assembly rates in seeded reactions, but only by a factor of 15, not 100 (Table 1). Substituting sonicated fibers for unfractured fibers produced no further increase (Table 1). Together with the data described above, these observations strongly suggest that assembly rates under these conditions approached a limit imposed by the time required for conformational conversion.

**A model for NM amyloid formation.** Our investigations of the S $\rightarrow$ A transition and its relation to assembly suggest a mechanism for the replication of NM's conformational information, which is the basis of its capacity to serve as a genetic element. This model, nucleated conformational conversion (NCC) (Fig. 1), incorporates aspects of NP and TA with additional features. Conformational conversion is nucleated by a complex of A-state proteins and is driven by assembly. Nuclei form by conformational rearrangements of less structured protein within the context of a structurally molten, oligomeric intermediate. When nuclei are present assembly proceeds rapidly, with less structured NM acquiring the A state through a templating or induced-fit mechanism at fiber ends. Other species might be competent for polymerization, but we suggest that assembly is most efficient with oligomers (31).

We propose that NM oligomers are initially micelle-like: They form through still fluid associations, involve variable stoichiometries, and are in equilibrium with monomers as well as smaller and larger complexes. Several lines of evidence directly support an on-pathway role for these unusual intermediates. Moreover, they provide a simple explanation for two aspects of the kinetic analysis that are otherwise baffling: (i) because overly large ineligible complexes increase proportionately with eligible complexes at higher concentrations, both the lag and the assembly phases show little variation in rate over a broad range of protein concentrations; and (ii) because oligomers are the limiting species for rapid assembly, as the number of nuclei increases, assembly rates are limited even when total soluble protein is in vast excess to fiber ends.

Notably, replication of structural information through an oligomeric intermediate was previously proposed for Sup35 on the basis of its genetic interaction with Hsp104. Hsp104 is a protein-remodeling factor thought to act by unfolding its substrates (32, 33). Either too little or too much Hsp104 cures cells of [PSI<sup>+</sup>] (2, 3, 34, 35). Such unusual dosage

relationships often reflect an imbalance in factors that form oligomeric species (36). If Hsp104 promotes oligomer formation by producing less-structured forms of Sup35, it would bypass a thermodynamic barrier in vivo that we have bypassed in vitro by starting with unfolded NM.

NM is an unusual protein in that it retains a

high degree of conformational flexibility (with a random-coil CD signal) for extended periods in aqueous buffers. As a monomer, NM may confront Levinthal's paradox; that is, it has too many accessible conformations to find a stable fold in a reasonable time frame (37). We suggest that oligomers alter the folding environment of NM polypeptides, allowing them to (i) slowly rearrange into structured nuclei themselves, (ii) undergo conformational conversion upon association with preformed nuclei, and (iii) progress to species not yet locked into a rigid structure yet capable of more rapid assembly when nuclei are added. Many other polypeptides have the capacity to form self-assembling  $\beta$ -sheet fibers, ranging from those associated with human protein-misfolding diseases (38) to synthetic peptides used in materials science applications (39). It will be of great interest to determine if NCC is applicable to other members of this diverse group of polypeptides.

**Fig. 4.** Analysis of the lag and assembly phases. NM (5  $\mu$ M) resuspended in CRBB in the absence (A, B, E, and F) or presence (C and D) of sonicated fibers. (A) Inverse lag time ( $L_T$ ) versus log of monomer concentration (41). (Left) Ellipticity at 220 nm was monitored in reactions stirred with a magnetic bead in 1-cm quartz cuvettes containing 2 ml of NM solutions at 0.1, 0.15, 0.2, 0.5, 1, and 5  $\mu$ M in a Jasco J715 Spectropolarimeter. Slope = 0.4. (Right) CR binding for reactions at 1.1, 2.5, 5, 10, 20, and 50  $\mu$ M NM, quantified as in Fig. 3. Slope = 0.7. (B) Assembly time ( $A_T$ ) versus concentration for undisturbed reactions (hours) (●) or reactions rotated as in Fig. 2 (min) (○). (C) Ellipticity at 220 nm, monitored for undisturbed NM (5  $\mu$ M) with 0.1, 0.15, 0.2, 0.5, 1, 2, 4, and 7% (w/w) sonicated fibers added just before the start of data collection. Rates were calculated by fitting to a single exponential equation with GraFit 4 (Erithacus Software Limited, Surrey, UK, 1998). (D) Ellipticity at 220 nm, monitored as in (C) with sonicated fibers (0.15% w/w) added immediately (left) or after 8 hours at 25°C (right). Rate =  $0.017 \pm 0.001$  mdeg/min (left),  $0.527 \pm 0.060$  mdeg/min, and  $0.013 \pm 0.007$  mdeg/min (right). Data were collected immediately after addition of fibers. (Top) Kinetics were fit to single or double exponential equations as in (C). (Bottom) Residuals (Res) from the fitting. (E) Light scattering as in Fig. 3 immediately after dilution into buffer. Lane 1: NM, 25°C, CRBB; lane 2: NM, 4°C, CRBB; lane 3: NM, 25°C, 1 M NaCl, 5 mM potassium phosphate (pH 7.4); and lane 4: His<sub>10</sub>-tagged NM, 25°C, CRBB. (F) Unseeded reactions were performed and analyzed by CR binding as in Fig. 3. Conditions: (□) NM, 4°C, CRBB; (○) His<sub>10</sub>-tagged NM, 25°C, CRBB; (●) NM, 25°C, CRBB; (△) NM, 25°C, 5 mM potassium phosphate (pH 7.4)–1 M NaCl. Each experiment was performed three times with similar results.

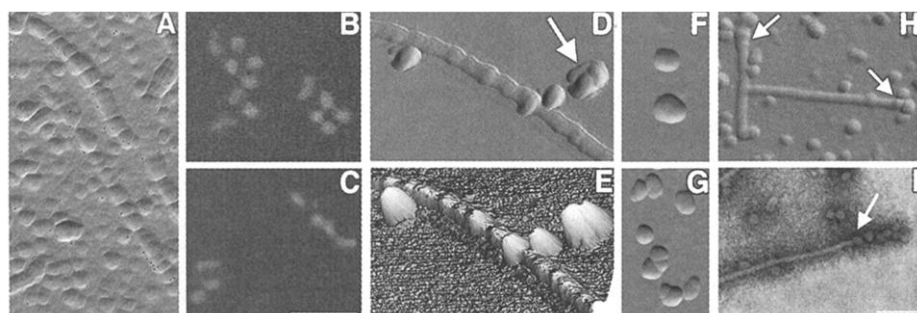
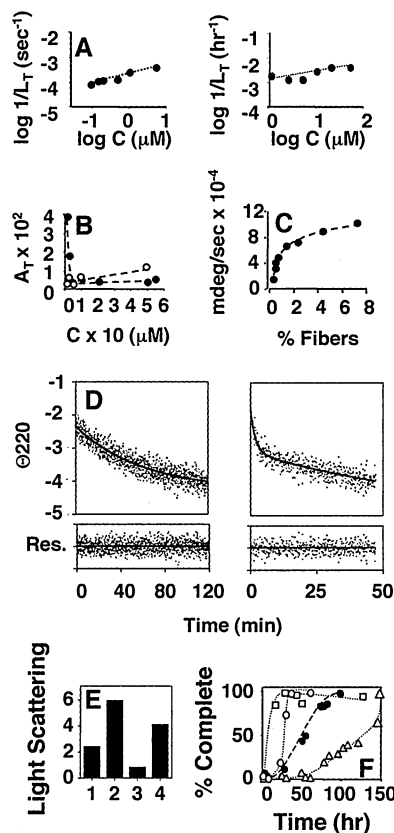


**Fig. 5.** Microscopy analysis of NM assembly. (A) AFM deflection image of a carbon-coated grid prepared for TEM as in Fig. 2. The sample is from an unseeded reaction of His<sub>10</sub>-tagged NM after 20 hours of incubation in CRBB at 25°C, imaged in contact mode with a Digital Instruments Nanoscope III by using standard 200- $\mu$ m thin-legged Si<sub>3</sub>N<sub>4</sub> cantilevers. (B and C) STEM images of His<sub>10</sub>-tagged NM 4 hours after resuspension in CRBB obtained as described (42). (D) AFM deflection image of unseeded reactions of untagged NM after overnight incubation at 25°C. Fifty microliters of a 1:500 dilution of 5  $\mu$ M untagged NM in CRBB was spotted onto 15-mm mica disks and adsorbed for 30 s. Disks were washed with 100  $\mu$ l of CRBB and then 100  $\mu$ l of water (three times). Samples were air-dried and imaged as in (A). (E) AFM surface plot of the height data in (D). (F to H) AFM deflection images as in (D) of an unseeded reaction of His<sub>10</sub>-tagged NM after ~5 hours of incubation at 25°C. (I) TEM image of His<sub>10</sub>-tagged NM 3 hours after resuspension in CRBB as in Fig. 2. Bars, 100 nm.

#### References and Notes

1. B. Cox, *Heredity* **20**, 505 (1965).
2. Y. O. Chernoff, S. L. Lindquist, B. Ono, S. G. Inge-Vechtormov, S. W. Liebman, *Science* **268**, 880 (1995).
3. M. M. Patino, J. J. Liu, J. R. Glover, S. Lindquist, *Science* **273**, 622 (1996).
4. S. V. Paushkin, V. V. Kushnirov, V. N. Smirnov, M. D. Ter-Avanesyan, *EMBO J.* **15**, 3127 (1996).
5. J. R. Glover *et al.*, *Cell* **89**, 811 (1997).
6. S. V. Paushkin, V. V. Kushnirov, V. N. Smirnov, M. D. Ter-Avanesyan, *Science* **277**, 381 (1997).
7. A. H. DePace, A. Santoso, P. Hillner, J. S. Weissman, *Cell* **93**, 1241 (1998).
8. J. J. Liu and S. Lindquist, *Nature* **400**, 573 (1999).
9. J. Griffith, *Nature* **215**, 1043 (1967).
10. Y. Uratani, S. Asakura, K. Imahori, *J. Mol. Biol.* **67**, 85 (1972).
11. S. B. Prusiner, *Science* **216**, 136 (1982).
12. G. H. Beaven, W. B. Gratzler, H. G. Davies, *Eur. J. Biochem.* **11**, 37 (1969).
13. J. Hofrichter, P. D. Ross, W. A. Eaton, *Proc. Natl. Acad. Sci. U.S.A.* **71**, 4864 (1974).
14. J. T. Jarrett and P. T. Lansbury Jr., *Cell* **73**, 1055 (1993).
15. M. Sunde *et al.*, *J. Mol. Biol.* **273**, 729 (1997).
16. The quantity of fibers added to the assembly reactions as seed was undetectable by the methods we used.
17. T. R. Serio *et al.*, data not shown.
18. Sonicated fibers remained resistant to SDS solubilization and chymotrypsin, sedimented, bound Congo red and ANS, retained  $\beta$ -sheet-rich CD spectrum, and scattered light (17).
19. <sup>125</sup>I-immunoblotting allowed quantitation of chymotrypsin sensitivity; however, the resistance of NM to digestion with chymotrypsin was confirmed by Coomassie Brilliant Blue staining (17).
20. In three separate unseeded reactions, CR binding reached the half-maximal point at 53, 45, and 51 hours. In each case, the other traits appeared coincidentally with CR-binding capacity (17).
21. L. S. Stryer, *J. Mol. Biol.* **13**, 482 (1965).
22. The existence of an ordered hydrophobic surface has also been detected by birefringence of CR bound to NM fibers (A. G. Cashikar and S. L. Lindquist, unpublished observation). It is unclear whether the CR and ANS binding sites are the same.
23.  $L_T$  is defined as the period of time in which CR binding is less than 10% maximal.  $A_T$  is defined as the interval of time required for CR binding to proceed from 10 to 90% maximal levels.
24. J. D. Harper and P. T. Lansbury Jr., *Annu. Rev. Biochem.* **66**, 385 (1997).
25. It could not be tested below this concentration because protein was lost to the sides of the tubes (17).

26. D. L. Caspar, *Biophys. J.* **32**, 103 (1980).
27. For additional data, see Science Online ([www.sciencemag.org/feature/data/1052183.shl](http://www.sciencemag.org/feature/data/1052183.shl)).
28. Based on a comparison of light-scattering intensities for His<sub>10</sub>-tagged NM in the presence of 50  $\mu$ M ZnCl<sub>2</sub>, which converts most of the protein to oligomeric species (17).
29. Fibers were stable to 8 M urea and 2% SDS, whereas the monomer:oligomer equilibrium was altered even by changes in temperature and salt concentration.
30. By TEM, even the overnight rotation (60 rpm) did not fracture mature fibers. In addition, rotated fibers seeded the fibrillization of fresh NM at a rate similar to that of seeding by unagitated fibers (17).
31. The slow phase in preincubated reactions may represent either the addition of monomers or the rate at which the intermediate is formed.
32. J. R. Glover and S. Lindquist, *Cell* **94**, 73 (1998).
33. E. U. Weber-Ban, B. G. Reid, A. D. Miranker, A. L. Horwich, *Nature* **401**, 90 (1999).
34. S. Lindquist and E. C. Schirmer, in *Molecular Chaperones and Folding Catalysts. Regulation, Cellular Function and Mechanisms*, B. Bukau, Ed. (Harwood, Amsterdam, 1999), pp. 347–380.
35. T. R. Serio and S. L. Lindquist, *Annu. Rev. Cell Dev. Biol.* **15**, 661 (1999).
36. Our data, therefore, indicate that the effects of Sup35 concentrations on [PSI<sup>+</sup>] induction in vivo reflect alterations in the ratio of the prion protein to Hsp104 and other cellular factors, rather than in the intrinsic folding and conversion properties of Sup35.
37. K. A. Dill, *Protein Sci.* **8**, 1166 (1999).
38. P. T. Lansbury Jr., *Proc. Natl. Acad. Sci. U.S.A.* **96**, 3342 (1999).
39. K. H. Mayo, *Trends Biotechnol.* **18**, 212 (2000).
40. T. R. Serio, A. G. Cashikar, J. J. Moselehi, A. S. Kowal, S. L. Lindquist, *Methods Enzymol.* **309**, 649 (1999).
41. Because of sensitivity limitations in CR binding at low protein concentration and CD at high protein concentrations, both methods were used across the broad concentration range tested. Further, stirred reactions for CD proceeded faster than unstirred reactions for CR binding.
42. J. S. Wall and J. F. Hainfeld, *Annu. Rev. Biophys. Biophys. Chem.* **15**, 355 (1986).
43. We thank T. Scheibel for plasmid pJC25NMstop (6798) and advice; M. Simon, B. Lin, J. Wall, and the Brookhaven National Laboratory for assistance with STEM; members of the Lindquist lab for comments and discussion; S. Xu and B. Bevis for assistance with AFM; and the National Institutes of Health (GM025874, P41-RR017777, GM57840), the Howard Hughes Medical Institute, U.S. Department of Energy, Office of Biological and Environmental Research, the Keck Foundation (991705), Materials Research Science and Engineering Centers (DMR 9808595), and the Cancer Fund of the Damon Runyon-Walter Winchell Foundation (DRG-1436) for financial support.

15 May 2000; accepted 3 July 2000

## REPORTS

## Hydrological Impact of Heinrich Events in the Subtropical Northeast Atlantic

Edouard Bard,<sup>1\*</sup> Frauke Rostek,<sup>1</sup> Jean-Louis Turon,<sup>2</sup>  
Sandra Gendreau<sup>2</sup>

Reconstructing the impact of Heinrich events outside the main belt of ice rafting is crucial to understanding the underlying causes of these abrupt climatic events. A high-resolution study of a marine sediment core from the Iberian margin demonstrates that this midlatitude area was strongly affected both by cooling and advection of low-salinity arctic water masses during the last three Heinrich events. These paleoclimatic time series reveal the internal complexity of each of the last three Heinrich events and illustrate the value of parallel studies of the organic and inorganic fractions of the sediments.

High-resolution paleoclimatic records show that the glacial climate was far more variable than previously thought. Studies of North Atlantic sediments show that the circulation of the surface and deep waters was repeatedly perturbed by massive surges and melting of icebergs. Although most researchers would agree that these so-called Heinrich (H) events originated from the Laurentide ice sheets (1–6), there is growing controversy about the precise behavior of other ice sheets during these events [see recent works on lithological indices (7, 8) and studies based on the Sr-Nd isotopic signatures of ice-rafted detritus (IRD) (9, 10)].

The influence of Heinrich events has sometimes been invoked to explain unusual high-frequency climatic events at low latitudes [e.g., (11)]. Abrupt decreases of sea surface temperature (SST) in phase with Heinrich events were detected in sediments of the Bermuda Rise (12) and the Mediterranean Sea (13). Further south, the tropical western Atlantic apparently warmed during H1 and the Younger Dryas (YD) (14). The strong, direct effect of melting icebergs is generally thought to be restricted to a North Atlantic belt between 40°N and 55°N, where IRD forms distinct layers in the sediments (15). The occurrence and climatic impact of H events are still poorly documented in the northeast Atlantic, especially at subtropical latitudes.

To reveal the impact of H events on the northeast Atlantic, we focused our study on the paleoceanographic variability in a midlatitude core from the Iberian margin (SU8118 located at 37°46'N, 10°11'W and 3135 m depth) (Fig. 1). One of the main advantages of using SU8118 is that it is one of the best-dated cores available for the last

deglaciation (16). These sediments are characterized by a high sedimentation rate (>20 cm/1000 years during the glacial and deglacial sections) which has been constrained by numerous <sup>14</sup>C accelerator mass spectrometry (AMS) ages and stable isotope records (17).

SST changes were reconstructed with the alkenone unsaturation ratios (Fig. 2B and Web table 1) (18, 19), and counts of IRD (Fig. 2B and Web table 1) (18, 20) and magnetic susceptibility (MS; Fig. 2B) (21) were used to identify transported sediments. The alkenone temperature estimates are on the order of 18°C during the last 5000 years, which is between the modern annual mean (17.5°C) and the SST during summer months (19°C) when most of the local primary productivity takes place. With an average sampling resolution of ~250 years, the alkenone-SST record shows the classical climate history of the Late Glacial: the Holocene starts at 11,500 calendar years before present (cal yr B.P.), the YD event is centered at about 12,000 cal yr B.P., and the Allerød-Bølling interstadial occurs between 13,000 and 15,000 cal yr B.P. Interestingly, the LGM in the strictest sense (21,000 ± 2000 cal yr B.P.) is a rather mild period, with SST on the order of 13°C, i.e., about 5°C lower than modern SST. In addition, the glacial period is characterized by a rather large variability with abrupt cold spells centered at about 16,000, 23,500, 26,000, and 31,000 cal yr B.P.

Figure 2B shows the IRD counts and the MS record which can be used to identify detrital material usually attributed to H events. These are clearly expressed in both records between 18,000 and 15,500 cal yr B.P. for H1 and between 26,000 and 23,000 cal yr B.P. for H2. The MS and mineralogical records (20) also suggest that each of these two events were complex and characterized by two depositional phases centered at 16,000 (H1a) and 17,500 (H1b) cal yr B.P. for H1 and at 23,500 (H2a) and 25,000 (H2b) cal yr B.P. for H2. Our results

<sup>1</sup>Centre Européen de Recherche et d'Enseignement en Géosciences de l'Environnement (CEREGE), UMR 6635, CNRS, and Université d'Aix-Marseille III, Euro-pôle de l'Arbois, 13545 Aix-en-Provence cedex 4, France. <sup>2</sup>Département de Géologie et Océanographie (DGO), UMR EPOC 5805, CNRS and Université de Bordeaux I, Avenue des Facultés, 33405 Talence cedex, France.

\*To whom correspondence should be addressed. E-mail: bard@cerege.fr